Journal of Environmental Chemical Engineering 11 (2023) 109060

Contents lists available at ScienceDirect

Journal of Environmental Chemical Engineering

journal homepage: www.elsevier.com/locate/jece

MgO-containing porous carbon spheres derived from magnesium lignosulfonate as sustainable basic catalysts

M. García-Rollán, F.J. García-Mateos, R. Ruiz-Rosas, J.M. Rosas, J. Rodríguez-Mirasol [*,1], T. Cordero

Universidad de Málaga, Departamento de Ingeniería Química, Andalucía Tech., Campus de Teatinos s/n, 29010 Málaga, Spain

ARTICLE INFO

Editor: Chao He

Keywords:
Lignin
Activated carbon
Basic catalyst
Dehydrogenation
CO2 gasification
Magnesium nanoparticles

ABSTRACT

The presence of alkalis in lignosulfonate allows an easy preparation of sustainable MgO-containing carbon catalysts with surface basicity by carbonization of magnesium lignosulfonate and/or further partial gasification of the produced char with CO_2. Carbon spheres with different chemical and physical properties were obtained from lignosulfonate treated at temperatures ranging from 500 to 900 ºC. Carbonization at 900 °C generates hollow porous carbon spheres (pore volume of 0.20 cm^3/g and apparent surface area of 465 m^2/g) with magnesium content of 12%. A kinetic study of CO_2 gasification of the carbon spheres obtained at 900 °C at temperatures in the range of 700 – 800 °C revealed that the gasification rate can be accurately described by the random pore model up to conversion values of 0.5. Based on this study, in order to develop additional porosity on the carbon spheres obtained at 900 °C, a partial gasification with CO_2 at 750 °C for 30 min was carried out, reaching surface areas higher than 700 m^2/g and 15.3% of Mg loading, with an overall preparation yield of 30%. All the obtained carbon materials were tested as catalyst for 2-propanol decomposition, showing a high selectivity to acetone, evidencing the basic character of these carbon catalysts. The highest activity and selectivity were shown by the CO_2-activated carbon spheres (conversion and acetone selectivity higher than 90% at 420 °C), indicating that magnesium lignosulfonate is an attractive raw material for the preparation of sustainable carbon catalysts for biorefinery applications.

1. Introduction

As a way to mitigate the global warming effects caused by the overuse of fossil fuels, new policies around the world encourages the sustainable production of biofuels and chemicals from renewable sources. The production processes that are currently deployed for achieving these goals fit into the biorefinery framework. Biorefineries are industrial complexes where different sustainable processes for enabling biomass transformation in different high added value products are implemented [1].

Lignin is one of the three main constituents, together with cellulose and hemicellulose, of the lignocellulosic biomass. It is the biopolymer that holds together the structure of tree biomass, filling the spaces between cellulose and hemicellulose in the plants cell walls. It can be considered as a three-dimensional, heterogeneous macromolecule formed by the polymerization of three types of alcohols, known as monolignols. Lignin is mainly obtained as a co-product in the papermaking industry [2] and can be isolated during the production of second generation bio-ethanol from biomass waste [3]. Nowadays, lignin is mostly burned in the mills for energy generation.

In order to minimize its combustion, previous studies have proposed alternative methods to valorize this lignocellulosic by-product [4,5]. Pyrolysis is one of the main thermochemical processes to obtain valuable products from lignin [6]. By this process, products can be obtained in the form of gas, composed of CO, CO_2, H_2 and incondensable hydrocarbons; liquids that are mainly formed by phenol derivatives; and a carbonaceous material known as char. The latter can be used as an enhanced solid fuel or as a precursor in the production of activated carbons. In this sense, slow pyrolysis of lignin is known to produce a solid residue which generally possesses narrow microporosity narrow microporosity [7,8], which can be further enlarged by means of physical or chemical activation, obtaining the resulting activated carbon (AC)

* Corresponding author.
E-mail address: mirasol@uma.es (J. Rodríguez-Mirasol).
[1] Permanent address: Universidad de Málaga, Departamento de Ingeniería Química, Andalucía Tech., Escuela de Ingenierías Industriales, Campus de Teatinos s/n, 29010 Málaga, Spain

https://doi.org/10.1016/j.jece.2022.109060
Received 2 August 2022; Received in revised form 2 November 2022; Accepted 25 November 2022
Available online 26 November 2022

[9–11].

Gasification is also an important thermochemical process and its application over a carbonaceous material can be focused on the production of a high added value gaseous product, such as synthesis gas (syngas), a mixture of CO and H_2 [12,13], or alternatively (by partial gasification) also in the production of a solid with enhanced physicochemical properties, such as activated carbons [14,15]. The main gasifying agents are diluted O_2 [16,17], steam [18] and CO_2 [9,19], in order of decreasing reactivity. This last compound can be obtained by CO_2 capture from the exhaust gases from combustion chambers or even directly from the air, which would provide further environmental advantages to this gasification process. In this case, CO_2 gasification of lignocellulosic biomass would be able to provide carbon materials with high added value from a renewable and sustainable feedstock and a CO stream, a fuel gas with a high heating value, whose productions would help to strength the circular bioeconomy.

On the other hand, the inorganic matter present in the lignocellulosic biomass, as Na, K, Ca, or Mg [19–24], can act as a gasification catalyst allowing the use of milder reaction conditions, i.e., reducing the gasification time and temperature. In this context, chars from pyrolysis of lignin with high ash content can be successfully used as activated carbon precursors [25].

In order to ensure that gasification proceeds with generation of porosity, it is required a knowledge of the gasifying agent reactivity, the reaction mechanism and the gasification rate of char. With this goal, the kinetic study of carbons gasification has been already carried out applying ideal models that have been proposed in literature [26–28].

In addition, the presence of inorganic matter in the biomassic materials may be also of great interest for the possible direct generation of catalyst-containing activated carbons, due to its high dispersion and concentration on the surface of these materials. For instance, different basic catalysts based on alkaline, alkaline-earth and transition metal oxides can be used in different reactions such as alcohol dehydrogenation [29–31], transesterification reactions [32], aldol condensations [33], the Meerwein-Ponndorf-Verley reaction [34] or the Michael reaction [35].

In this sense, lignosulfonates, which is the lignin with the highest commercial implementation, have been already reported as precursor in the preparation of carbon materials, useful in many applications such as adsorbent [36], supercapacitors [37] or sulfur donor/acceptor in lithium-sulfur batteries [38]. However, to the best of our knowledge, the use of chars obtained by slow pyrolysis of magnesium lignosulfonate as activated carbon precursor for the preparation of basic carbon catalysts has not been reported in the literature. Following the circular economy principles, the use of lignin, an abundant by-product of paper making industry and lignocellulosic biorefinery, as raw material to produce sustainable carbon-based catalysts would enhance the sustainability of these industries by decreasing the waste generation and increasing the recycling products and materials.

Thus, this work reports the preparation of MgO-containing porous carbon materials through the carbonization of the most commercialized lignin, magnesium lignosulfonates, followed by CO_2 partial gasification. The porosity and surface chemistry of chars have been characterized, whereas the kinetics of CO_2 gasification of the char with the larger porosity development has been studied to understand the process of generating additional porosity. The resulting MgO-containing carbon materials have been tested as basic catalyst in an alcohol dehydrogenation reaction the decomposition of 2-propanol, a well-known test to evaluate the acidity/basicity of heterogeneous catalyst, yielding propylene by dehydration reaction (acid character) or acetone by dehydrogenation reaction (basic character).

2. Materials and methods

2.1. Materials

Magnesium-lignosulfonate produced from Eucalyptus softwood by sulfite isolation method, where $MgCO_3$ had been used to obtain the cooking liquor, was supplied by Sappi Biotech GmbH, Stockstadt, Germany. HCl (≥ 37%, Fluka), 2-propanol (≥ 99.9%, Carlo Erba) and N_2 5.0, CO_2 4.5 and He 5.0 from Linde.

2.2. Carbon materials preparation

Magnesium-lignosulfonate was used as carbon precursor. In the carbonization step, magnesium-lignosulfonate was submitted to a thermal treatment at different temperatures (500, 700 and 900 °C), under constant N_2 flow (150 $Ncm^3\ min^{-1}$), with a heating rate of 10 °C min^{-1} and maintaining the final temperature for 2 h. After the thermal treatment, the carbon material obtained at 900 °C was partially gasified under continuous CO_2 flow (150 $Ncm^3\ min^{-1}$) at 750 ºC for 30 min. The nomenclature used for the carbon materials (chars) was L (for magnesium-lignosulfonate) followed by a number, which refers to the thermal treatment temperature. The activated carbon obtained by partial gasification with CO_2 was labelled with the letter G, L900G.

2.3. Reactivity studies

The gasification reactivity of char was studied using a CIElectronics thermogravimetric system for the carbon material prepared at 900 °C (L900). In order to assess the reactivity of the char, isothermal experiments were carried out at different temperatures, where around 15 mg of sample with a particle size of 150 μm were heated at 15 °C min^{-1} in a nitrogen flow (150 $Ncm^3\ min^{-1}$), up to temperatures from 725 °C to 800 °C. When the sample reached the required temperature, the flow was switched to 150 $Ncm^3\ min^{-1}$ of CO_2 and remained constant until the end of the process. The conversion values in ash free basis were referred to the starting sample weight after reaching the operating temperature. Assuming spherical particles and that kinetic control of the reaction is achieved, the isothermal conversion rates can be described using different kinetic models. However, the random pore model proposed by Bhatia and Perlmutter is one of the most used for estimating gasification rates [28]:

$$\frac{dx}{dt} = (k' \cdot P_{CO_2}^{m}) \cdot (1-x) \cdot (1 - \varphi \cdot Ln(1-x))^{\frac{1}{2}} = k \cdot (1-x) \cdot (1 - \varphi \cdot Ln(1-x))^{\frac{1}{2}} \quad (1)$$

Here, x stands for the conversion, k' is the reaction rate constant ($atm^{-m}\ s^{-1}$) and P_{CO_2} is the CO_2 partial pressure (1 atm), m is the CO_2 reaction order. It is assumed that CO_2 pressure remains constant and grouped into the kinetic constant, k (s^{-1}), as the CO_2 molar flow rate is several orders of magnitude higher than the reaction rate. Finally, φ is true structural parameter, related to the density of the solid and the starting porosity of the unreacted sample [28]. Taking into account the Arrhenius law, the previous equation could be rewritten as follows:

$$\frac{dx}{dt} = k_0 \cdot e^{-\frac{Ea}{RT}} \cdot (1-x) \cdot (1 - \varphi \cdot Ln(1-x))^{\frac{1}{2}} \quad (2)$$

Where Ea stands for the activation energy (kJ mol^{-1}), k_0 represents the preexponential factor (s^{-1}), R is the ideal gas constant ($8.314 \cdot 10^{-3}$ $kJ \cdot mol^{-1}\ K^{-1}$) and T is the gasification temperature (K), which is considered to remain constant during the whole experiment.

The kinetic parameters Ea, k_0 and φ, were evaluated by simultaneous non-lineal least-square fitting of the experimental conversion vs time profiles, recorded at 725, 750, 775 and 800 °C, by the minimization of the following objective function:

$$\text{O.F.} = \sqrt{\sum \left(X(t)_{TB} - X(t)_{model}\right)^2} \quad (3)$$

In it, $X(t)_{TB}$ represents the experimental conversion vs time profile and $X(t)_{model}$ stands for the conversion obtained by the numerical solution in time of the ordinary differential equation (Eq. 2). The minimization of Eq. 3 was implemented in Matlab 2021b using a Levenberg-Marquart algorithm.

2.4. Carbon materials characterization

The porous texture of the carbon materials was studied by N_2 adsorption-desorption at − 196 °C and CO_2 adsorption at 0 °C, by using a Micromeritics ASAP2020 equipment. Previous to the analysis, the samples were submitted to a degassing process for at least 8 h at 150 °C. From N_2 adsorption isotherms, the specific surface area (A_{BET}) was obtained using the BET equation following the criteria proposed by Rouquerol for the selection of the fitting region. Moreover, the micropore volume (V_s) and external surface area (A_s) were calculated using the α_s method. Finally, the mesopore volume (V_{mes}) was estimated following the Gurvich rule and calculated as the difference between the adsorbed volume at relative pressure of 0.98 and the micropore volume (V_s). Dubinin-Radushkevich method was applied to the CO_2 adsorption isotherms for the determination of the narrow micropore volume (V_{DR}) and surface area (A_{DR}). Pore size distribution is obtained from the N_2 and CO_2 adsorption isotherms by using the 2D-NLDFT heterogeneous surface model [39].

X-ray photoelectron spectroscopy (XPS) was carried out to analyse the surface chemistry of lignosulfonate and carbon materials by using a 5700 C model Physical Electronics equipment with MgKα radiation (1253.6 eV). The maximum of the C1s peak has been set to the XPS photoemission energy of the C-C bond (284.5 eV) and used as internal reference to correct the position of the other peaks. Temperature programmed desorption (TPD) technique was utilized in order to study the nature and amount of the oxygen surface groups of the carbon materials. TPD experiments were carried out loading 100 mg of dry sample in a quartz reactor and heating from room temperature to 900 °C at 10 °C min^{-1} in a N_2 flow of 100 Ncm^3 min^{-1}. The quantities of CO and CO_2 desorbed were monitored in a non-dispersive infrared (NDIR) gas analyzer, Siemens ULTRAMAT 23. The total amount of CO or CO_2 evolved during the entire analysis were calculated by integrating the area under the evolution profiles of the two gases. With the aim of knowing the inorganic composition of the ash in the samples, X-Ray Fluorescence (XRF) analysis were carried out in an atomic fluorescence wavelength dispersive spectrometer THERMO ARL PERFORM'X equipment.

The morphology of the carbon materials was studied by scanning electron microscopy (SEM) using a JSM 6490LV JEOL microscope working at 20 kV. An energy-dispersive X-ray analyses (SEM-EDX) was performed to study the atomic distribution of the carbon surfaces using an Oxford instrument model 7573 equipment. The X-ray diffraction (XRD) patterns of the carbon materials were recorded in an EMPYREAN diffractometer (PANalytical), over a 2θ range of 5–80° during 30 min with 45 kV, 40 mA and a CuKα1,2 (1.5406 Å) monochromatic radiation. Transmission Emission microscopy (TEM) images were taken using a FEI Talos F200X microscope at 200 kV. Image mapping distribution of the main elements present in the catalyst were recorded using Energy Dispersive X-Ray (EDX) detector.

2.5. 2-propanol decomposition

The acid or basic character of the obtained carbons was studied by 2-propanol decomposition. It is known that 2-propanol is dehydrated on catalytic acid sites, producing propylene, or it is dehydrogenated on basic sites, generating acetone. In a typical run, 100 mg of catalyst was introduced in a quartz fixed bed microreactor (4 mm i.d.) located in a vertical furnace. 2-propanol was introduced into the set up using a syringe pump (Cole Parmer® 74900–00–05 model), and He flow was used as inert carrier. A total gas flow of 100 Ncm^3 min^{-1} was used in all the experiments. The space time used in each experiment was $W/F_{02\text{-propanol}}$= 73 g s $mmol^{-1}$. The reactant and products involved in the reaction were measured at the reactor outlet by gas chromatography with PPQ, 5 A molsieve and Wax columns installed in a 490 micro-GC. In order to avoid their condensation, all the pipelines were heated to 130 °C. The 2-propanol conversion and the selectivity to different hydrocarbon products were defined by the following expressions:

$$X_{2p} = \frac{F_0 - F}{F_0} \quad (4)$$

$$S_i = \frac{F_i}{\sum F_i} \quad (5)$$

Where X_{2p} is 2-propanol conversion and S_i stands for the selectivity to the different hydrocarbon products. F_0 and F are the 2-propanol molar flow fed to the system and that at the reactor outlet stream and F_i is the molar flow of the *i* product in the outlet stream.

3. Results and discussion

3.1. Characterization of lignosulfonate and chars

Table 1 shows the pyrolysis yields, ash content and ultimate analysis of the chars prepared between 500 and 900 °C. For the sake of comparison, ash content and ultimate analysis of the magnesium lignosulfonate (L) was also included. The preparation yields and the elemental composition summarized in Table 1 are reported on dry and ash free basis (d.a.f.). The ash content of the raw material (about 7%) is higher than that of the most technical lignins [17,40], only surpassed by Kraft lignin [41]. The main inorganic components detected by XRF are Mg, followed by K and Ca. Fe, Mn and P were also detected, though in much lower amounts. The content of these elements in the lignin will increase in the produced chars, making them promising candidates for the preparation of activated carbons by physical activation with CO_2, since alkali metals are the most active catalysts for carbon gasification [42], with the catalytic activity increasing with atomic weight [43]. Another interesting feature of L as carbon precursor is the large presence of S (higher than 5%, Table 1) due to the isolation method used in its extraction. This high sulfur content can be also an additional advantage because sulfur-doped carbon materials have recently gained lots of attention for their potential in energy and catalytic applications [44].

Focusing on the chars, Table 1 shows that the preparation yields decrease with temperature, from 42.7% at 500 °C to a value of 28.0% for the char prepared at 900 °C. These preparation yields are higher than the ones reported with other lignocellulosic biomass sources [17,45,46], due to a larger generation of pyrolytic solid residue produced by lignin than that produced by hemicellulose and cellulose [47]. Nevertheless, the carbonization yield is somehow lower than those registered for Kraft, Alcell, and other technical lignins (yields of 40–45% at 800 °C) [41,48,49]. The presence of certain alkalis species probably promotes gasification of the char through the formation of carbonates during pyrolysis, which are decomposed as CO_2 at higher temperatures [50]. In this sense, high values of inorganic matter are observed in the chars, showing a clear increase in ash content with the preparation temperature, due to the increasing contribution of devolatilization process.

A reduction in the concentration of heteroatoms in the ultimate analysis of the chars can be observed (H, O and S), close to an increment in C content with the temperature until 900 °C. In addition, this tendency can be also associated to decomposition of inorganic carbonates and sulfates and aromatic condensation during carbonization at higher temperatures [51].

Fig. 1 shows the N_2 adsorption-desorption isotherm at − 196 °C and

Table 1
Preparation yields, ash content and ultimate analyses of lignin and different chars.

Samples	Preparation Yields (% d.a.f.#)	Ash (%)	XRF (%)			Ultimate Analysis (% d.a.f.)				
			Mg	K	Ca	C	H	N	S	O*
L	–	6.8	3.2	0.3	0.2	37.6	5.3	0.1	5.3	51.7
L500	42.7	17.8	8.6	0.9	0.4	67.6	3.9	0.3	3.4	24.8
L700	31.7	25.6	12.7	1.3	0.6	81.7	1.5	0.2	3.7	13.0
L900	28.0	28.8	14.4	1.5	0.7	88.8	0.9	0.2	2.5	7.5
L900G	20.1	33.1	15.3	2.2	0.9	83.6	1.7	0.3	0.2	11.1

#d.a.f.: dry, ash free basis
*O: calculated by difference

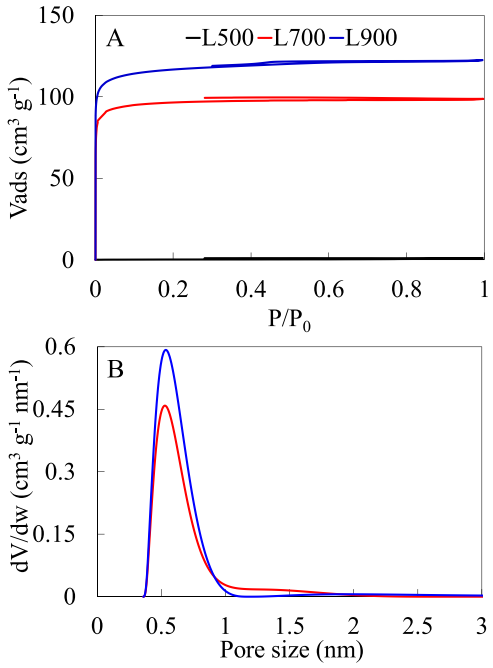

Fig. 1. N_2 adsorption-desorption isotherms obtained at − 196 °C (A) and Pore Size Distribution (B) of samples obtained at different carbonization temperatures.

the pore size distribution of the carbonized samples at different temperatures. The char obtained at 500 °C present an almost negligible N_2 adsorption in the entire range of relative pressure of the isotherm, typical of nonporous solids. At preparation temperatures higher than 700 °C, a type I isotherm, typical of microporous solids, was observed. The char prepared at 900 °C showed an increase of the nitrogen uptake at low relative pressures, indicating a significant microporosity development, which is related to volatilisation and condensation reactions occurring to a greater extent at higher temperatures, close to the decomposition of the magnesium sulfonate present in the lignin, taking place at temperatures from 550 °C [52,53]. Apparent surface areas from 390 to 465 $m^2\ g^{-1}$ and micropore volume from 0.15 to 0.19 $cm^3\ g^{-1}$ are obtained by direct carbonization of magnesium lignosulfonate at 700 and 900 °C, respectively. In addition, the development of porosity is significantly higher than those prepared from a sodium-lignosulfonate at the same carbonization temperatures (A_{BET} of 8–30 $m^2\ g^{-1}$), which required a further washing step to release the porosity by the removal of the inorganic matter [41].

The adsorption of CO_2 at 0 °C is useful in the case of materials with very narrow microporosity (<0.7 nm) [54]. In this sense, the relation between V_s/V_{DR} can be used to analyse the microporous sizes. Values of this relation lower than 1 indicate the main presence of narrow microporosity in the sample (<0.7 nm), while values higher than 1 evidence the predominance of wide micropores (>0.7 nm). In this case, V_s/V_{DR} values close to 1 (Table 2) are obtained, suggesting that average pore size is close to 0.7 nm for L700 and L900 samples. The NLDFT pore size distribution obtained for L700 by combination of the N_2 and CO_2 adsorption isotherms [39] confirmed the presence of a unimodal narrow distribution of micropores (pore width between 0.35 and 1.05 nm) centered at 0.55 nm. Increasing the carbonization temperature produces additional development of the micropores with sizes between 0.6 and 0.7 nm.

Fig. 2 represents the CO and CO_2 evolved profiles during the temperature programmed desorption (TPD) of the chars. This technique is widely used to characterize the oxygen surface groups that decompose as CO and/or CO_2 with temperature [55]. In general, the amount of CO and CO_2 evolved during the TPD profiles are very high (see the quantities as inset in Fig. 2. A and B). The total oxygen contents, estimated as $CO + 2{\cdot}CO_2$ for L500, L700 and L900 are 14.8, 9.7 and 6.1 wt%, would lead to the conclusion of the presence of large amounts of typical surface (-carbon) oxygen groups. However, the presence of inorganic matter could be behind part of this high CO and CO_2 evolution [23].

In the case of the CO L500 TPD profile (Fig. 2. A), the peak observed at approximately 400–600 °C can be related to the thermal decomposition of anhydride groups, which also release CO_2 in equimolar ratio [55], as deduced from Fig. 2.B. The evolved CO at temperatures of 600–700 °C can be attributed to the decomposition of phenol groups, which are abundant in the composition of all lignins and also in lignosulfonates and it is very possible that some of them have remained stable on the surface of the char prepared at 500 °C (L500) [56–58]. The large CO evolution observed at 700 °C could be initially related to the decomposition of ether or quinones [55]. However, it can be also related to the presence of inorganic matter. In this sense, Kapteijn et al. compared the total amount of oxygen desorbed during TPD of acid functionalized commercial activated carbon impregnated with different alkali metal carbonates using a metal/carbon atomic ratio of 0.2 [59]. They found that the oxygen metal ratios were related, showing large CO_2 evolution profiles linearly related to alkali content and equimolar CO/Metal ratios. In addition, the gasification of the char with CO_2 evolved during the carbonization process could be also taking part at these temperatures, releasing two CO molecules through the following mechanism [59,60]:

$$MO + CO_2(g) \leftrightarrow MO.O + CO(g) \quad (6)$$

$$MO.O + C \leftrightarrow MO + C(O) \quad (7)$$

$$C(O) \leftrightarrow CO(g) \quad (8)$$

Where M stands for alkali and alkaline earth metals, such as K, whose presence has been confirmed by XRF and XPS (see Table 3).

The CO_2 desorption at temperatures from 200 to 400 °C in Fig. 2. B is traditionally ascribed to carboxylic acid surface groups. However, the generation of such a high concentration of carboxylic acid functionalities without the use of a surface oxidation treatment with HNO_3 or any other strong oxidizing agent [61,62] is very unlikely. In fact, magnesium carbonates are known to decompose at temperatures around 350 °C [63], so a relevant fraction of the CO_2 released at this temperature range

Table 2
Textural parameters obtained from N_2 and CO_2 isotherms at − 196 °C and 0°C, respectively, of the carbon materials.

Samples	N_2 isotherm					CO_2 isotherm		V_s/V_{DR}
	A_{BET} (m^2/g)	A_s (m^2/g)	V_s (cm^3/g)	V_{meso} (cm^3/g)	$V_{0.995}$ (cm^3/g)	A_{DR} (m^2/g)	V_{DR} (cm^3/g)	
L500	1	1	< 0.01	< 0.01	< 0.01	20	0.01	0.0
L700	390	1	0.15	< 0.01	0.15	420	0.17	0.9
L900	465	3	0.19	< 0.01	0.19	450	0.18	1.1
L900G	720	25	0.36	0.03	0.39	455	0.18	2.0

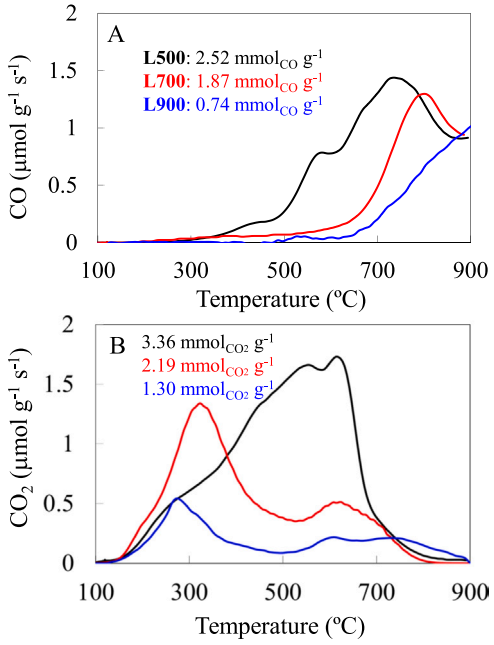

Fig. 2. CO (A) and CO_2 (B) evolved as a function of temperature during TPD of chars prepared at different temperatures (L500, L700 and L900).

Table 3
Mass surface concentration (%) determined by XPS analyses of the magnesium lignosulfonate and the corresponding chars.

Samples	XPS Surface Composition (wt%)				
	C	O	Mg	S	K
L	47.3	39.6	6.5	6.6	< 0.1
L500	51.9	29.4	13.2	3.7	1.8
L700	66.9	16.4	13.0	2.4	1.3
L900	66.0	18.1	10.9	2.2	2.8
L900G	70.1	19.5	8.6	1.8	< 0.1

can be related to the decomposition of magnesium carbonates. It is also worth noting that the CO_2 evolution in the 500–700 °C region of sample L500 is higher than expected for chars prepared at similar temperatures [41,64]. With the aim of discerning whether the CO_2 evolution comes from the ash or the decomposition of the surface acidic groups, the char was submitted to an acid wash with 10% HCl. The CO_2-TPD profile of the ash-free char, Fig. S1, revealed an important reduction of the evolved CO and CO_2 amounts at this temperature range, highlighting that evolution of CO_2 between 400 and 650 °C in L500 proceeds, mainly, from reactions involving the inorganic elements found in this sample. For instance, the carboreduction of magnesium sulfone groups (in the temperature range of 500–700 °C) present in the char, which produced the evolution of huge amounts of CO_2 [65].

In accordance with the latter finding, L700 and L900, which were carbonized at temperatures above the carboreduction of magnesium sulfonate, show a much lower CO_2 release at 400–650 °C during TPD, with only two main peaks at 300 °C (decomposition of carboxylic acids) and 650 °C (decomposition of lactones and/or anhydrides), although it could be also related to decomposition of some carbonate surface groups [64]. CO evolution profile of L700 reveals the presence of a well-defined peak at 750 °C, probably related to the decomposition of ethers and/or quinones. These surface groups are negligible, when carbonization proceeds at 900 °C, in a similar way to that reported for other carbonaceous materials [66]. In this sample, L900, highly stable quinone and carbonyl groups are only found, which decompose as CO at temperatures over 800 °C [66]. Thus, the high total CO and CO_2 evolved amounts (insert of Fig. 2) suggests that all the carbon materials are rich in oxygenated surface groups.

XPS analyses were carried out to determine the surface chemical composition and the oxidation states of their elements. Table 3 compiles the mass surface composition of L sample and their corresponding chars. It can be observed that C surface concentration increases with the carbonization temperature, in agreement with the elemental analyses. O (%) content shows a large decrease when carbonization temperature increases from 500 to 700 ºC, probably related to condensation reactions and/or to the carbothermal reduction of magnesium sulfonates (as can be deduced from the TPD results of sample L700). The comparison of sulfur content of L900G determined by ultimate analysis and XPS analyses suggest that sulfur is not homogeneously distributed on the bulk and is mainly concentrated on the outer surface. It is also worth noting that sulfur values as high as 2.0 wt% are still found on the surface of the char prepared at 900 °C, L900, proving the potentiality of producing chars with a relatively high and stable S-content by a simple, well-known and already mature technology from a sustainable precursor, magnesium lignosulfonate, which opens up the possibilities of applications, such as in heterogeneous catalysis and in lithium-sulfur batteries [29,30,32–35,44]. The surface concentration of magnesium almost doubles after lignin carbonization (see Mg content values for L and L500 in Table 1). However, potassium migrates to the surface of the char after carbonization, reaching concentration values higher than those predicted from the initial content of potassium in the raw material, shown in Table 1. Both magnesium and potassium elements are bonded to sulfones and organic groups, such as carboxylic acids, in the original lignosulfonate. The carbonization process delivers a fine distribution of Mg on the whole surface of the obtained chars, as indicated by the values of the relation between the content of Mg measured by XPS (Table 3) and that measured by XRF (Table 1), decreasing from 1.5 to 0.8 with increasing carbonization temperature (from 500 to 900 °C, respectively). However, the higher mobility of potassium [42] probably enhances the migration of this component to the surface of the char.

The XPS spectra were examined to analyse the main oxidation states of the elements. Fig. 3 presents the detailed S2p and Mg2p spectra, while C1s and O1s XPS regions are provided in Fig. S2 and discussed in the supplementary file. The S2p spectrum of the lignosulfonate, Fig. 3. A, only shows a wide peak. This peak was deconvoluted by considering a separation value of the doublet of 1.18 eV and its majority contribution is found at 168 eV. This value is typical of the sulfite groups (C-S═O) [67,68] present in lignosulfonates. In this sense, carbonization at 500 ºC is not able to modify the oxidation state of sulfur, which takes place at carbonization temperatures above 700 ºC, as can be seen in samples L700 and L900. In them, the remaining sulfur is in the form of sulfide (C-S-C) or thiol (C-S-H), detected in S2p spectrum at 163.7 and

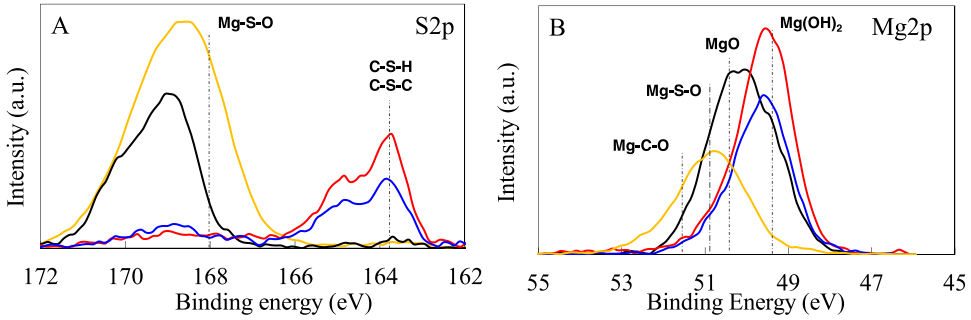

Fig. 3. XPS normalized spectra of L (yellow line), L500 (black line), L700 (red line) and L900 (blue line) samples.

163.8 eV, respectively [67,68]. Finally, focusing on the Mg2p spectrum of sample L, in Fig. 3. B, it can be seen a broad peak centered at 50.6 eV, typical for magnesium sulfonates [69]. The decomposition of the sulfonates groups during carbonization produces the conversion of magnesium into other species such as hydroxides, which shows a peak at 49.1 eV [70], present together with the sulfonates groups in sample L500. As carbonization temperature increases, most sulfone groups disappeared (Fig. 3. C) and, therefore, most of the magnesium is transformed into hydroxides or oxides (MgO shows a peak at 50.2 eV) in samples L700 and L900. Magnesium carbonates (which would present a peak at 51.3 eV [71]) has not been observed in any of the Mg2p spectra, neither in C1s spectra (Fig. S2. A; it should present a peak at 289.9 eV), which is somehow expected due to the low thermal stability of $MgCO_3$, which readily decomposed at 350 °C [63]. The C1s and O1.

The morphology and chemical composition of the carbonized chars were also examined by scanning electron microscopy and energy-dispersive X-ray spectroscopy. SEM images (Fig. 4) show that chars are composed of hollow spheres of diameters between 100 and 200 μm with smooth surface and a greatly reduced spherical wall thickness (between 5 and 25 μm). Similar morphology has been previously observed for carbon-derived sodium lignosulfonates but using multi-step and complex preparation procedures [37,72–75]. It is important to note

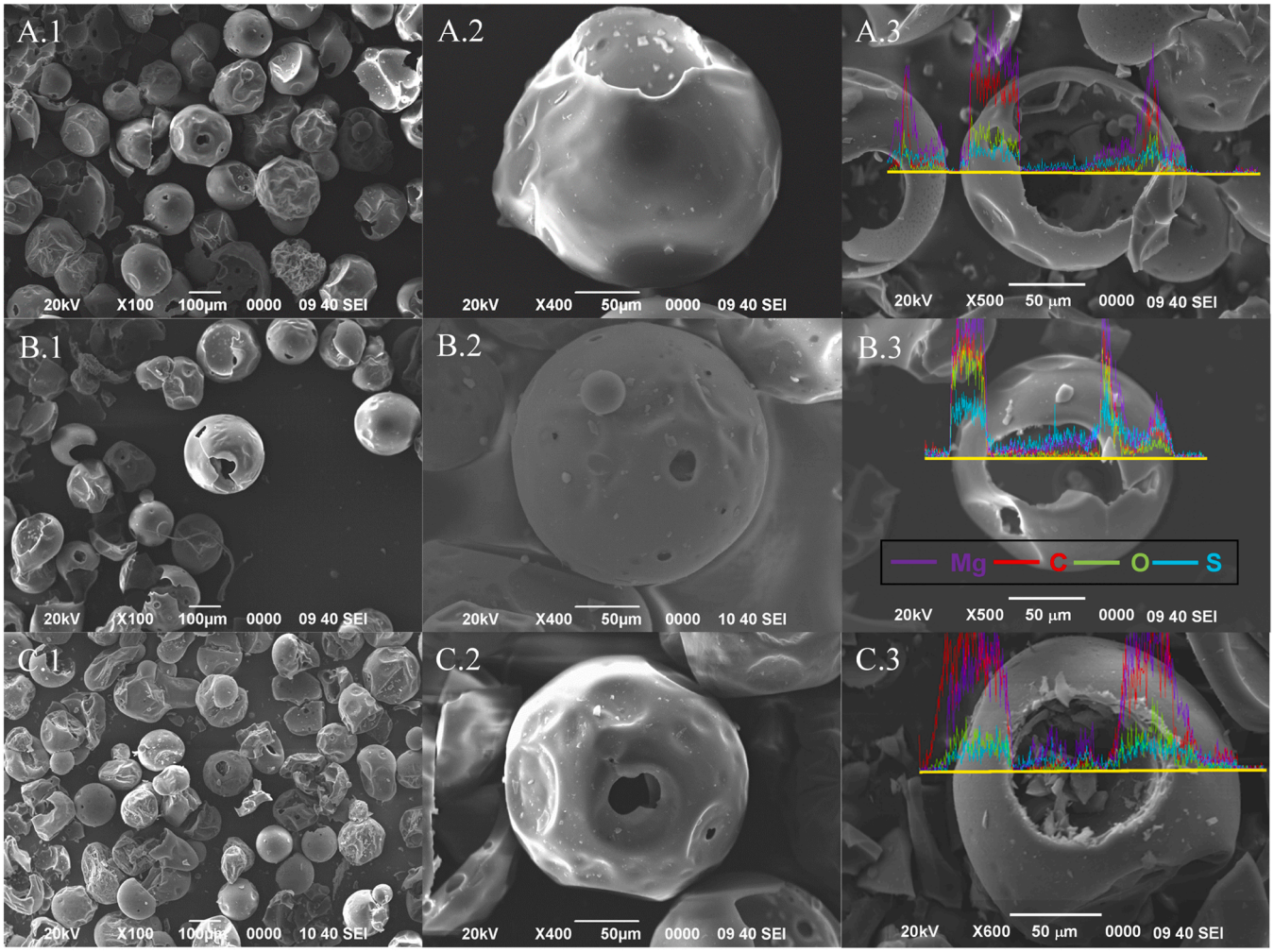

Fig. 4. Scanning electron micrographs of chars carbonized at 500 (A), 700 (B) and 900 (C) with different magnifications, (1) x 100 and (2) x 400 and EDX (3) with the elemental mapping of different atoms.

that the spherical morphology from the parent lignin is kept after carbonization. This is related to the high glass transition temperature of lignosulfonates [76] and associated to their high molecular weight, which makes this co-product a promising precursor of carbon materials with specific morphologies, without the need of further treatments. To the best of our knowledge, hollow sphere chars from magnesium lignosulfonates are here reported for the first time. EDX measurements, shown in Fig. 4. A.3, Fig. 4. B.3 and Fig. 4. C.3, point out that C, O, Mg and S are the main chemical species that the carbon spheres are composed of, which are homogenously distributed, in agreement with XRF and XPS results.

3.2. Kinetics of char gasification with CO_2

A kinetic study of the physical activation of L900 has been carried out with the aim of optimizing the preparation of an activated carbon by partial gasification of a magnesium lignosulfonate-derived char with carbon dioxide. L900 has been selected to be activated due to its higher amount of (catalytic) inorganic matter (Table 1) and largest microporosity development (Table 2), which enable a higher porosity growth and larger burn-off under milder conditions. Moreover, given that partial gasification requires high reaction temperatures, the use of a char obtained at temperatures above 800 °C is advisable for avoiding chemical and structural changes during the activation process, an approach commonly taken in similar works [9,46].

Fig. 5. A shows the conversion of L900 as a function of reaction time for the CO_2 gasification at temperatures ranging from 725 to 800 °C. Different kinetic models like the first and second order, random pore and shrinking core ones were tested to describe the conversion profiles, Table S1. The random pore model (RP) provides the most accurate prediction of the conversion versus time profiles (Fig. 5. A and S3), showing the lowest residual value (Table S2) and $R^2 = 0.989$. The activation energy predicted by this model, 185 kJ mol^{-1}, is in the range of those obtained for chars prepared from kraft lignin at 850 °C or the gasification of chars from eucalyptus wood prepared at 800 °C [24,77].

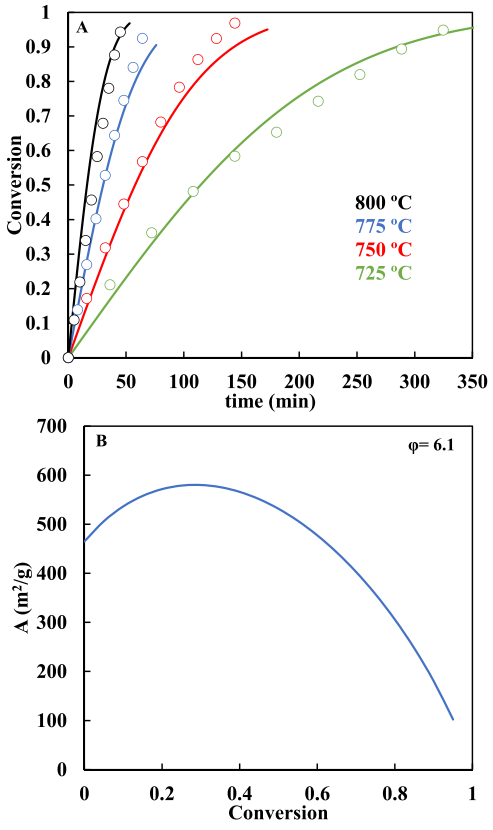

Fig. 5. Experimental (dots) and calculated by RP model (continuous lines) gasification conversion-time profiles of L900 at different temperatures (A). Evolution of apparent surface area of L900 during CO_2 gasification of L900 predicted by the RP model (B).

It is also worth noting that some deviation between the results predicted by the RP model and the intrinsic reactivity ($-\frac{dw}{dt}/w$) experimental data at conversions larger than 0.5 can be observed, Fig. S3. These deviations can be explained by the catalytic activity of potassium [77,78]. Even though magnesium concentration is at least 5 times higher, according to XPS (Table 2), magnesium is regarded as the less active alkaline earth metal for gasification. In fact, the decomposition temperatures of magnesium carbonate and hydroxide are below 350 °C, and once MgO is formed, it is so stable that a catalytic cycle as that described by Kapteijn et al. [22], cannot occur [42]. Contrarily, potassium is extensively reported as the most active gasifcation catalyst, with concentrations as low as 0.85 wt% being active for coal gasification [79]. It is expected that K/C atomic ratio increases as gasification proceeds, and therefore the contribution of the potassium catalyzed-reaction to the char reactivity may overcome the effect related to the modification of the active surface area described by RP model.

RP model considers a relationship between the gasification rate with conversion through the evolution of the surface area (A, in m^2/g) of the carbon material during the gasification process [28]:

$$\frac{dx}{dt} = k \cdot A \cdot (1 - x) \tag{9}$$

With the variation of the surface area being described as follows:

$$A = A_0 \cdot \sqrt{1 - \varphi \cdot Ln(1 - x)} \tag{10}$$

Where A_0 is the initial surface area of L900 sample. Fig. 5. B depicts the evolution of the apparent surface area with conversion predicted by RP model using the structural parameter value obtained from the model fitting ($\varphi = 6.1$) and the A_{BET} value reported in Table 2 (465 m g^{-1}) as A_0. As can be observed, RP model predicts a maximum development of surface area at conversion values of 25%, expecting a surface area value of 580 m^2 g^{-1}. In accordance to this finding, 25% of burn-off (BO) is selected for promoting the development of porosity without compromising the yield of the process and avoiding metal sintering [11]. To obtain this BO, an activation time of 30 min at 750 °C has been estimated from the RP (Eq. 2 solved with the kinetic parameters in Table S2). The activated carbon, produced under these conditions, has been labelled as L900G.

3.3. Characterization of CO_2 activated carbon spheres

Fig. 6 shows the N_2 adsorption-desorption isotherm at − 196 °C and the pore size distribution of samples L900 and L900G. Regarding the narrow microporosity measured by CO_2 adsorption at 0 °C, it can be highlighted that there are no differences between char and activated carbon (V_{DR}^{CO2} of 0.18 cm^3 g^{-1} in L900G). A similar behaviour on the development of porosity at low BO levels was also reported elsewhere [9,80]. The presence of narrow mesopores has been also confirmed by the NLDFT pore size distribution (Fig. 6. B). The PSD of char L900 for narrow micropores (<1 nm) is very similar to that of the corresponding activated carbon (L900G), due to the smooth conditions selected for the activation process. However, wider micropores and mesopores are generated, during activation, in L900G, with pore sizes ranging from 1.3 up to almost 6 nm.

Textural parameters have been calculated from the N_2 adsorption isotherm and are included in Table 2. Higher values of the specific surface area, micropore and mesopores volume were obtained for L900G in comparison to those for L900. It is remarkable that an increase in more than 50% in A_{BET} has been obtained only with a BO of 25% (overall yield of 30%). This increase is 25% higher than that predicted by RPM, probably due to the catalytic effect of potassium during the partial

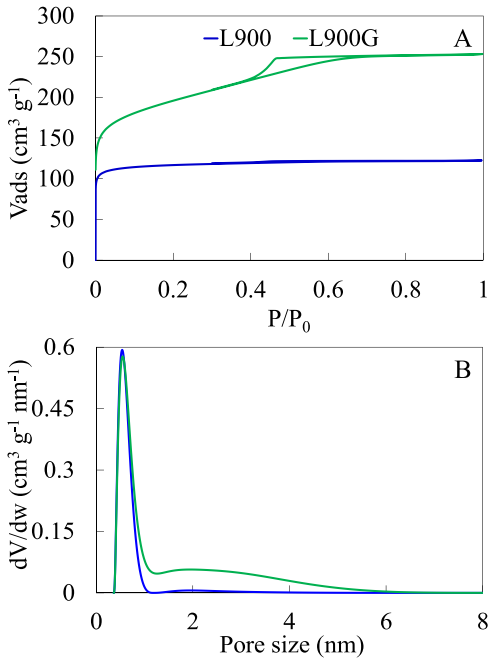

Fig. 6. N_2 adsorption-desorption isotherms obtained at − 196 °C (A), Pore Size Distribution derived from N_2 and CO_2 adsorption isotherms (B) of samples L900 and L900G.

gasification process. The A_{BET} and pore volume values are somehow similar to those obtained by chemical activation of kraft lignin with zinc chloride using mass ratio of 1 and carbonization temperature of 350 °C [81], or with H_3PO_4 with impregnation ratio of 2 and activation temperature of 350 °C [11]. The porosity development is also similar to that achieved in ACs from carbonized sodium lignosulfonates at 900 °C, where additional porosity had to be liberated by removing the inorganic matter through acid washing after carbonization [82]. However, the present AC has been prepared by a soft partial gasification process, consuming CO_2, a greenhouse gas, and without the use of chemical agents not very environmentally friendly.

XRF analyses show that the activation process slightly increases the magnesium content of the resulting sample, moving from 14.4 in L900 to 15.3 wt% in L900G, as a consequence of the carbon gasification, Table 1. The presence of potassium and calcium is also confirmed, though in lesser amounts (2.2 and 0.9 wt%, respectively). The surface concentration of elements was also determined by XPS, Table 3, showing a slight increase in O content (19.5%) for L900G compared to that of L900 and small decrease of that for Mg, S and C (8.7%, 1.8% 70.1% respectively). Detailed XPS analyses of L900G reveal that only minor differences are introduced on the surface chemistry of the sample after the activation process (see Fig. S4 and supplementary file for further details).

On the other hand, the TPD CO profile remains mostly unaltered, while there is a slight increase in the amount of CO_2 evolved at about 300 °C and over 750 °C (Fig. S5). This higher evolution could be related to the formation of carboxylic acid and lactone groups and also to the decomposition of alkali metal carbonates remaining on the surface of the activated carbon, such as K and Ca.

SEM micrographs of the L900G activated carbon show a slight erosion of the spherical morphology during the gasification process (Fig. 7), thus, the optimization of the activation conditions to fully maintain the spheres morphology could be analysed in a future study. There appears to be no sign of the development of surface roughness due to erosion by CO_2 gasification, confirming the smooth activation of the carbon spheres. The observed hollow sphere morphology is an interesting feature of this carbon material, which can avoid mass transfer limitations in adsorption and catalysis applications, due to the lower diffusional pathway for reagents through the thin walls of the spheres. The line energy-dispersive X-ray analysis (Fig. 7. C) reveals a similar surface composition and element distribution to that observed for L900. It is worth mentioning that magnesium species are homogeneously distributed throughout the hollow sphere. This fine distribution of Mg on L900G sample was also observed by TEM (Fig. 7. D). The images taken at different magnifications reveal the formation of a large number of evenly distributed crystalline nanoparticles, with average size of ca. 8 nm (Fig. 7. E). The measurements of the lattice in-plane distance (0.21 nm, see inset on Fig. 7. D) suggest the mainly presence of MgO crystallites. TEM-EDX analysis of the carbon spheres also confirms the fine distribution of magnesium oxide on this catalyst (Fig. 7. F).

In this line, XRD diffraction patterns of chars and CO_2-activated carbon (Fig. S6) also evidence the formation of crystalline MgO (Periclase structure, JCPDS card 45–946) in L700, L900 and L900G samples. The determination of the mean crystallite size using the Williamson-Hall method reveals that the average crystalline size slightly increases with carbonization temperature (4.8 nm for L700 vs 6.0 nm for L900). Activation with CO_2 seems to favour some sintering of MgO crystallites, although relatively small crystal sizes are maintained, with an average size of 8.5 nm, very similar to that determined by TEM analyses.

In summary, the characterization of L900G points out the possibility to prepare a carbon catalyst with a high content of nanometric MgO particles homogeneously distributed on the surface of hollow carbon spheres with a well-developed surface area, from a biorefinery by-product. In this sense, magnesium oxide is traditionally used as catalyst by itself or as a catalyst support in reactions where a basic active phase is required, as transesterification reactions [83]. However, it is known that its basic strength depends on the morphology of the catalyst particle and its surface area [84] and, thus, its activity.

In order to confirm the basic character of these carbon materials, the sphere-shaped lignosulphonate-derived activated carbon and chars obtained at different temperatures were tested as (dehydrogenation) catalysts for the decomposition of 2-propanol, a well-known model reaction used to characterize the acidity-basicity of solid catalysts.

3.4. 2-propanol dehydrogenation

Fig. 8. A represents the steady state conversion of 2-propanol at different reaction temperatures, for the different carbon catalysts, with a 2-propanol concentration of 2%v and a space time ($W/F_{0\ 2\text{-propanol}}$) of 73 g s $mmol^{-1}$. The 2-propanol conversion increases with the reaction temperature. The catalyst activity seems to increase with inorganic mater content and porosity development, which enables the access to the active sites of the catalysts. The highest activity was observed for L900G, which is able to decompose 2-propanol at 325 °C and achieves near complete conversion of alcohol at 420 °C, keeping the selectivity to the dehydrogenation product (acetone) higher than 90% in the full temperature range. Conversely, the parent char, L900, needs a higher temperature, ca. 50 °C, for achieving comparable conversion values, and the selectivity to acetone is not as high, showing selectivity to propylene values from 11% to 19%. The high activity of L900 and L900G samples can be associated to the preparation temperature of these samples. Thermal treatment at 900 °C promotes the generation of basic sites due to the formation of nanoparticles of MgO, which is related to the presence of O^{2-} ions of different coordination numbers [85]. Another advantage of using lignosulfonate as raw material arises from the presence of potassium. The higher activity of L900 and L900G samples can be also related not only to the occurrence of well-dispersed MgO, but also to the promoting effect of alkalis. It has been already stablished that Li, K and other alkalis promote higher basicity of MgO [86]. In this sense, Di Cosimo et al. stated that 2-propanol decomposition to acetone and propylene on alkali-modified MgO catalysts takes place via an E1cB mechanism in two parallel pathways, sharing a common 2-propoxy intermediate; in this mechanism, the intermediate-strength base sites promote acetone formation, whereas high-strength base sites selectively

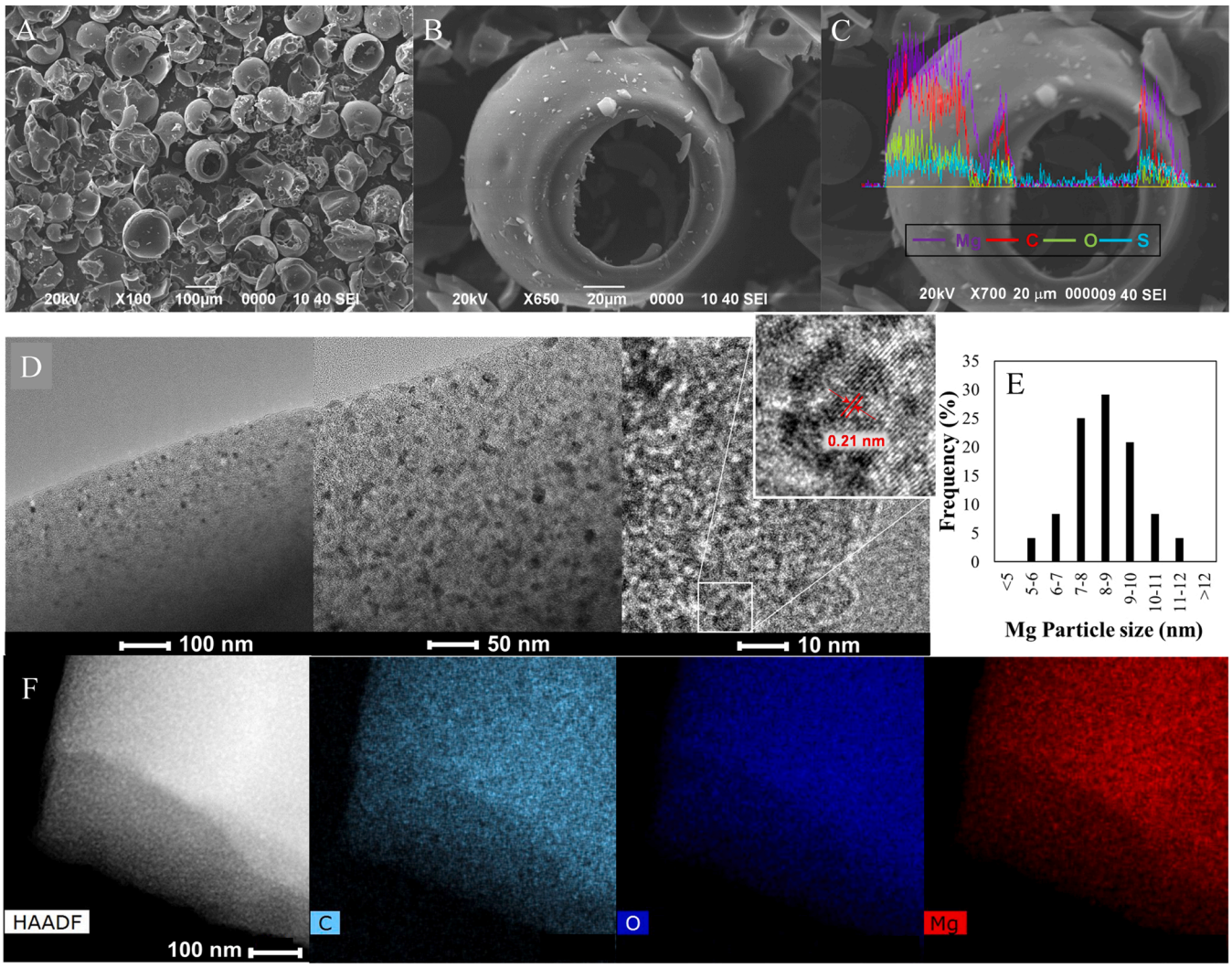

Fig. 7. Scanning electron micrographs of L900G (A) with 100 and (B) 650 magnifications. (C) EDX line mapping along the diameter of a L900G carbon sphere. (D) HR-TEM of L900G spheres at different magnifications; inset: planar distance of MgO crystal nanoparticle. (E) Size distribution of Mg nanoparticles estimated from TEM images. (F) HAADF and C, O and Mg EDX mapping images of L900G.

yield propylene [87], suggesting (in our case) that L900G mostly has an intermediate-strength basicity. In fact, pure MgO is reported to show IPA decomposition rate lower than other metal oxides, requiring the presence of promoters for enabling a relevant catalytic activity [88].

Inferior catalytic activity and lower selectivity towards dehydrogenation product were observed for L700 and specially for L500 chars. Again, the activity can be related to the Mg speciation, with magnesium hydroxide showing lower basicity character than low coordination O^{2-} anions and $Mg^{2+}O^{2-}$ pairs [85]. The distribution of magnesium species is mediated by the preparation temperature, due to magnesium hydroxide is transformed into its corresponding oxide as temperature increases. In addition, the origin of acidic properties in metal oxides are associated to overexposed metal cations and sulfate groups [88,89]. Therefore, the formation of propylene in L500 could be related to the presence of magnesium sulfate groups, which are decomposed into magnesium oxide at higher preparation temperatures (L900 and L900G samples). However, the contribution of surface oxygen groups of acid character (see TPD profiles, Fig. 2 and S4) cannot be discarded. These results suggest that L900G presents basic character with high catalytic activity due to the presence of well dispersed and highly accessible magnesium oxide.

Considering that the 2-propanol decomposition reaction takes place in an isothermal fixed bed reactor, in the absence of external mass transfer limitations, and assuming that follows a global first order kinetics, the integrated design equation of the reactor can be expressed as follows:

$$\ln\left(\frac{1}{1-X_{2p}}\right)=\frac{k}{\rho_L}\cdot\frac{P_0}{RT}\cdot\frac{W}{F_0} \tag{11}$$

Where X_{2p} is the alcohol conversion, k (s^{-1}) is the apparent rate constant, ρ_L (g cm^{-3}) is the catalytic bed density, P_0 (atm) is the 2-propanol partial pressure, R (atm cm^3 K^{-1} mol^{-1}) is the ideal gas constant, T (K) is the reaction temperature, W (g) is the catalyst weight and F_0 (mol cm^{-3}) is the inlet 2-propanol molar flow. The activation energy and the pre-exponential factor were obtained from the slope of the Arrhenius plot, represented in Fig. 9, being included on the figure as an inset. The corresponding activation energy values for this reaction on the chars are ranging between 58 and 68 kJ mol^{-1}, meanwhile the preexponential factor values are lower than 80 s^{-1}. These slight differences in the activation energy values of the chars can be associated to the porous texture of the materials. Thus, L500 and L700 present the lowest Ea. These catalysts also show a poor pore development, which could cause some internal diffusional limitations, diminishing the apparent activation energy. In the case of L900, with a wider pore size distribution, an increase in Ea was observed. Nevertheless, the kinetic parameters values obtained for L900G, which presents the highest pore development

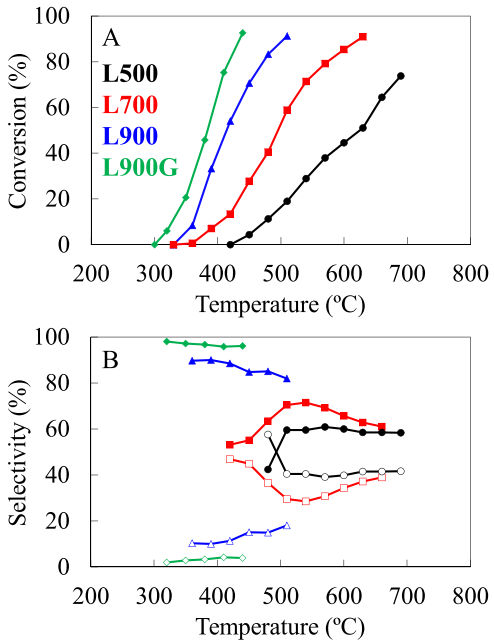

Fig. 8. Evolution of the steady-state conversions of 2-propanol (A) and selectivity to acetone (filled marks) and propylene (hollow marks) (B) with the temperature for all the carbonaceous materials.

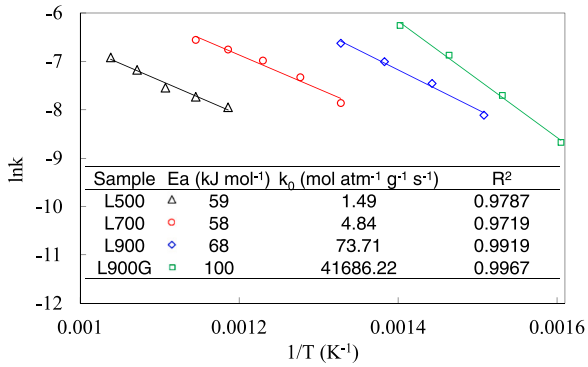

Fig. 9. Arrhenius plots for 2-propanol decomposition reaction using the different chars and the corresponding activated carbon, L900G. Inset: kinetic parameters.

(avoiding, in this case, mass transfer limitations problems) and number of active sites available, are the only ones comparable to those proposed in the literature for alkali-based catalysts supported on activated carbons [29,90]. The activity of L900G is also equivalent to that shown by Na-promoted MgO-SiO_2 catalyst at similar space times and reaction temperatures, but with higher selectivity towards the dehydration product [91]. However, L900G performs significantly better than others bulk MgO catalyst previously reported in literature, despite coming from a less sustainable and expensive synthesis process [92]. In this line, an alkali promoted MgO catalyst with high surface area, but prepared in a considerable higher number of steps, was tested at lower temperatures (260 °C) than those used in this work, but it showed lower activity (i.e. conversions from 1.6% to 13.8%) for similar selectivity to acetone (ca. 90%) [93]. In a similar way, Albuquerque et al. reported a Mg/CaO co-precipitated catalysts, which shows total selectivity towards acetone at mild conditions (350 °C), but with a low 2-propanol conversion (about 20%) [94]. On the contrary, Li et al. showed results on a MgO supported on mesoporous silica catalyst with full conversion at 350 ºC, but reporting low selectivity towards acetone (less than 2%) [95].

Thus, the results of the characterization and 2-propanol catalytic test suggest that it is possible to prepare a sustainable and highly active basic catalyst with hollow sphere morphology and thin wall thickness, which provides well-dispersed and highly accessible catalytic active sites, from magnesium lignosulfonate thorough a straightforward carbonization and CO_2 activation procedure.

4. Conclusions

Magnesium lignosulfonate is considered an ideal carbon precursor due to its abundance and sustainable origin. The presence of magnesium along with potassium enables the easy preparation of alkali promoted MgO base catalysts by carbonization and/or CO_2 activation. Carbonization at temperatures higher than 700 ºC enhances porosity development and generates magnesium oxide via decomposition of magnesium sulfonates, producing microporous hollow carbon spheres with well-dispersed magnesium oxide. The presence of potassium resulted to be essential for the subsequent CO_2 partial gasification process. The kinetic study of the gasification process revealed that random pore model can be used for predicting the activation process up to conversion values of 50%, from which the contribution of the catalytic activity of potassium generates strong deviations. Using the results derived from this model, MgO containing activated carbon spheres with well-developed porosity were prepared by partial gasification with CO_2 (B.O. 25%) at 750 °C for 30 min, reaching surface areas higher than 700 m^2/g and 15.3% of Mg loading, with an overall preparation yield of 30%. Finally, the 2-propanol decomposition model reaction confirmed the base behaviour of the resulting solids. The results suggest that activity of the carbon catalysts increases with MgO content and porosity development. Specifically, the activated carbon showed selectivity values to dehydrogenation product, acetone, higher than 90% in the whole range of reaction temperatures evaluated and conversions higher than 50% from 400 °C, achieving catalytic activity at least comparable to relevant MgO catalysts supported in metal oxides, with a less sustainable origin. These promising results confirms that basic catalysts can be obtained following this straightforward procedure from an industrial by-product of low cost, thus, reducing the total price of the catalyst preparation and increasing the sustainability.

CRediT authorship contribution statement

MGR, FJGM: Investigation, Formal analysis, Methodology, Visualization, Writing – original draft. **RRR, JMR:** Conceptualization, Methodology, Supervision, Validation, Writing – original draft, Writing – review & editing. **TCA, JRM:** Supervision, Writing – review & editing, Project administration, Funding acquisition.

Declaration of Competing Interest

The authors declare that they have no known competing financial interests or personal relationships that could have appeared to influence the work reported in this paper.

Data Availability

Data will be made available on request.

Acknowledgements

The authors wish to thank MICINN (RTI2018-097555-B-100) and Junta de Andalucía (UMA18-FEDERJA-110 and P18-RT-4592) for financial support. M.G.R. acknowledges the assistance of MICINN through an FPU Grant (FPU 18/01402). "Funding for open access charge: Universidad de Málaga / CBUA"

Appendix A. Supporting information

Supplementary data associated with this article can be found in the online version at doi:10.1016/j.jece.2022.109060.

References

[1] M.C. Gutiérrez, J.M. Rosas, M.A. Rodríguez-Cano, I. López-Luque, J. Rodríguez-Mirasol, T. Cordero, Strategic situation, design and simulation of a biorefinery in Andalusia, Energy Convers. Manag 182 (2019) 201–214, https://doi.org/10.1016/J.ENCONMAN.2018.12.038.

[2] P. Sannigrahi, Y. Pu, A. Ragauskas, Cellulosic biorefineries-unleashing lignin opportunities, Curr. Opin. Environ. Sustain 2 (2010) 383–393, https://doi.org/10.1016/j.cosust.2010.09.004.

[3] J. Zakzeski, P.C.A. Bruijnincx, A.L. Jongerius, B.M. Weckhuysen, The catalytic valorization of lignin for the production of renewable chemicals, Chem. Rev. 110 (2010) 3552–3599, https://doi.org/10.1021/cr900354u.

[4] K. Barta, T.D. Matson, M.L. Fettig, S.L. Scott, A. v Iretskii, P.C. Ford, Catalytic disassembly of an organosolv lignin via hydrogen transfer from supercritical methanol, Green Chem. 12 (2010) 1640–1647, https://doi.org/10.1039/c0gc00181c.

[5] R.K. Chowdari, S. Agarwal, H.J. Heeres, Hydrotreatment of kraft lignin to alkylphenolics and aromatics using Ni, Mo, and W phosphides supported on activated carbon, ACS Sustain Chem. Eng. 7 (2019) 2044–2055, https://doi.org/10.1021/acssuschemeng.8b04411.

[6] F. Xu, Q. Lu, K. Li, T.T. Zhu, W.K. Wang, Z.H. Hu, Green synthesis of magnetic mesoporous carbon from waste-lignin and its application as an efficient heterogeneous Fenton catalyst, J. Clean. Prod. 285 (2021), 125363, https://doi.org/10.1016/J.JCLEPRO.2020.125363.

[7] P.J.M. Suhas, M.M.L. Carrott, Ribeiro Carrott, Lignin - from natural adsorbent to activated carbon: a review, Bioresour. Technol. 98 (2007) 2301–2312, https://doi.org/10.1016/j.biortech.2006.08.008.

[8] O.N. Baklanova, G. v Plaksin, V.A. Drozdov, V.K. Duplyakin, N. v Chesnokov, B. N. Kuznetsov, Preparation of microporous sorbents from cedar nutshells and hydrolytic lignin, Carbon 41 (2003) 1793–1800, https://doi.org/10.1016/S0008-6223(03)00149-0.

[9] J. Rodriguez-Mirasol, T. Cordero, J.J. Rodriguez, Preparation and characterization of activated carbons from eucalyptus kraft lignin, Carbon 1 (1993) 87–95, https://doi.org/10.1016/0008-6223(93)90160-C.

[10] V. Fierro, V. Torné-Fernández, D. Montané, A. Celzard, Adsorption of phenol onto activated carbons having different textural and surface properties, Microporous Mesoporous Mater. 111 (2008) 276–284, https://doi.org/10.1016/j.micromeso.2007.08.002.

[11] E. Gonzalez-Serrano, T. Cordero, J. Rodriguez-Mirasol, L. Cotoruelo, J. J. Rodriguez, Removal of water pollutants with activated carbons prepared from H_3PO_4 activation of lignin from kraft black liquors, Water Res. 38 (2004) 3043–3050, https://doi.org/10.1016/J.WATRES.2004.04.048.

[12] F. Yan, S. Yi Luo, Z. Quan Hu, B. Xiao, G. Cheng, Hydrogen-rich gas production by steam gasification of char from biomass fast pyrolysis in a fixed-bed reactor: Influence of temperature and steam on hydrogen yield and syngas composition, Bioresour. Technol. 101 (2010) 5633–5637, https://doi.org/10.1016/j.biortech.2010.02.025.

[13] A.S. Al-Rahbi, P.T. Williams, Hydrogen-rich syngas production and tar removal from biomass gasification using sacrificial tyre pyrolysis char, Appl. Energy 190 (2017) 501–509, https://doi.org/10.1016/j.apenergy.2016.12.099.

[14] H. Marsh, F. Rodríguez-Reinoso, Activation Processes (Thermal or Physical), in: Activated Carbon, Elsevier Science & Technology, London, (2006) 243–321. https://doi.org/10.1016/B978–008044463-5/50019–4.

[15] F. Rodriguez-Reinoso, M. Molina-Sabio, M.T. Gonzalez, The use of steam and CO_2 as activating agents in the preparation of activated carbons, Carbon 33 (1995) 15–23, https://doi.org/10.1016/0008-6223(94)00100-E.

[16] L.R. Radovic Jr., P.L. Walker, R.G. Jenkins, Importance of carbon active sites in the gasification of coal chars, Fuel 62 (1983) 849–856, https://doi.org/10.1016/0016-2361(83)90041-8.

[17] J.M. Rosas, R. Ruiz-Rosas, J. Rodríguez-Mirasol, T. Cordero, Kinetic study of the oxidation resistance of phosphorus-containing activated carbons, Carbon 50 (2012) 1523–1537, https://doi.org/10.1016/j.carbon.2011.11.030.

[18] S.T. Chaudhari, A.K. Dalai, N.N. Bakhshi, Production of hydrogen and/or syngas (H2 + CO) via steam gasification of biomass-derived chars, Energy Fuels 17 (2003) 1062–1067, https://doi.org/10.1021/EF030017D.

[19] J. Rodríguez-Mirasol, T. Cordero, J.J. Rodríguez, CO_2-reactivity of eucalyptus kraft lignin chars, Carbon 31 (1993) 3–61, https://doi.org/10.1016/0008-6223(93)90155-4.

[20] A. Linares-Solano, C.S.M. de Lecea, D. Cazorla-Amorós, J.P. Joly, H. Charcosset, Nature and structure of calcium dispersed on carbon, Energy Fuels 4 (2002) 467–474, https://doi.org/10.1021/EF00023A011.

[21] M.C. Román-Martínez, D. Cazorla-Amorós, A. Linares-Solano, C.S.M. de Lecea, Carbon dioxide hydrogenation catalyzed by alkaline earth- and platinum-based catalysts supported on carbon, Appl. Catal. A Gen. 116 (1994) 187–204, https://doi.org/10.1016/0926-860X(94)80289-0.

[22] F. Kapteijn, G. Abbel, J.A. Moulijn, CO_2 gasification of carbon catalysed by alkali metals: Reactivity and mechanism, Fuel 63 (1984) 1036–1042, https://doi.org/10.1016/0016-2361(84)90184-4.

[23] F. Kapteijn, J.A. Moulijn, Kinetics of the potassium carbonate-catalysed CO_2 gasification of activated carbon, Fuel 62 (1983) 221–225, https://doi.org/10.1016/0016-2361(83)90203-X.

[24] J. Rodríguez-Mirasol, T. Cordero, J.J. Rodríguez, Activated carbons from CO_2 partial gasification of Eucalyptus Kraft lignin, Energy Fuels 7 (1993) 133–138, https://doi.org/10.1021/ef00037a021.

[25] J. Rodríguez-Mirasol, T. Cordero, J.J. Rodríguez, Preparation and characterization of activated carbons from eucalyptus kraft lignin, Carbon 31 (1993) 87–95, https://doi.org/10.1016/0008-6223(93)90160-C.

[26] J. Szekely, J.W. Evans, A structural model for gas-solid reactions with a moving boundary, Chem. Eng. Sci. 25 (1970) 1091–1107, https://doi.org/10.1016/0009-2509(70)85053-9.

[27] D.T. Lacey, J.H. Bowen, K.S. Basden, Theory of noncatalytic gas-solid reactions, Ind. Eng. Chem. Fundam. 4 (2002) 275–281, https://doi.org/10.1021/I160015A007.

[28] B. Feng, S.K. Bhatia, Variation of the pore structure of coal chars during gasification, Carbon 41 (2003) 507–523, https://doi.org/10.1016/S0008-6223(02)00357-3.

[29] J. Bedia, J.M. Rosas, D. Vera, J. Rodríguez-Mirasol, T. Cordero, Isopropanol decomposition on carbon based acid and basic catalysts, Catal. Today 96 (2010) 89–96, https://doi.org/10.1016/j.cattod.2010.04.043.

[30] K.I. Shimizu, K. Sugino, K. Sawabe, A. Satsuma, Oxidant-free dehydrogenation of alcohols heterogeneously catalyzed by cooperation of silver clusters and acid-base sites on alumina, Chem. A Eur. J. 15 (2009) 2341–2351, https://doi.org/10.1002/chem.200802222.

[31] E. Simón, J.M. Rosas, A. Santos, A. Romero, Study of the deactivation of copper-based catalysts for dehydrogenation of cyclohexanol to cyclohexanone, Catal. Today 187 (2012) 150–158, https://doi.org/10.1016/J.CATTOD.2011.10.010.

[32] T.F. Dossin, M.F. Reyniers, G.B. Marin, Kinetics of heterogeneously MgO-catalyzed transesterification, Appl. Catal. B 62 (2006) 35–45, https://doi.org/10.1016/j.apcatb.2005.04.005.

[33] G. Zhang, H. Hattori, K. Tanabe, Aldol addition of acetone, catalyzed by solid base catalysts: magnesium oxide, calcium oxide, strontium oxide, barium oxide, lanthanum (III) oxide and zirconium oxide, Appl. Catal. 36 (1988) 189–197, https://doi.org/10.1016/S0166-9834(00)80114-1.

[34] F. Wang, N. Ta, W. Shen, MgO nanosheets, nanodisks, and nanofibers for the Meerwein-Ponndorf-Verley reaction, Appl. Catal. A Gen. 475 (2014) 76–81, https://doi.org/10.1016/j.apcata.2014.01.026.

[35] B.M. Choudary, K.V.S. Ranganath, U. Pal, M.L. Kantam, B. Sreedhar, Nanocrystalline MgO for asymmetric Henry and Michael reactions, J. Am. Chem. Soc. 127 (2005) 13167–13171, https://doi.org/10.1021/ja0440248.

[36] D. Saha, N. Mirando, A. Levchenko, Liquid and vapor phase adsorption of BTX in lignin derived activated carbon: Equilibrium and kinetics study, J. Clean. Prod. 182 (2018) 372–378, https://doi.org/10.1016/J.JCLEPRO.2018.02.076.

[37] J. Pang, W. Zhang, H. Zhang, J. Zhang, H. Zhang, G. Cao, M. Han, Y. Yang, Sustainable nitrogen-containing hierarchical porous carbon spheres derived from sodium lignosulfonate for high-performance supercapacitors, Carbon 132 (2018) 280–293, https://doi.org/10.1016/j.carbon.2018.02.077.

[38] L. Li, L. Huang, R.J. Linhardt, N. Koratkar, T. Simmons, Repurposing paper by-product lignosulfonate as a sulfur donor/acceptor for high performance lithium–sulfur batteries batteries, Sustain Energ. Fuels 2 (2018) 422–429, https://doi.org/10.1039/c7se00394c.

[39] J. Jagiello, C. Ania, J.B. Parra, C. Cook, Dual gas analysis of microporous carbons using 2D-NLDFT heterogeneous surface model and combined adsorption data of N_2 and CO_2, Carbon 91 (2015) 330–337, https://doi.org/10.1016/j.carbon.2015.05.004.

[40] S. Constant, H.L.J. Wienk, A.E. Frissen, P. de Peinder, R. Boelens, D.S. van Es, R.J. H. Grisel, B.M. Weckhuysen, W.J.J. Huijgen, R.J.A. Gosselink, P.C.A. Bruijnincx, New insights into the structure and composition of technical lignins: a comparative characterization study, Green. Chem. 18 (2016) 2651–2665, https://doi.org/10.1039/c5gc03043a.

[41] F.J. García-Mateos, I. Moulefera, J.M. Rosas, A. Benyoucef, J. Rodríguez-Mirasol, T. Cordero, Alcohol dehydrogenation on kraft Lignin-derived chars with surface basicity, Catalysts 7 (2017) 308–321, https://doi.org/10.3390/catal7100308.

[42] R.A. Arnold, J.M. Hill, Catalysts for gasification: a review, Sustain Energ. Fuels 3 (2019) 656–672, https://doi.org/10.1039/c8se00614h.

[43] R. Meijer, M. Weeda, F. Kapteijn, J.A. Moulijn, Catalyst loss and retention during alkali-catalysed carbon gasification in CO_2, Carbon 2 (1991) 929–941, https://doi.org/10.1016/0008-6223(91)90171-E.

[44] W. Kiciński, M. Szala, M. Bystrzejewski, Sulfur-doped porous carbons: synthesis and applications, Carbon 68 (2014) 1–32, https://doi.org/10.1016/j.carbon.2013.11.004.

[45] J.M. Rosas, J. Bedia, J. Rodríguez-Mirasol, T. Cordero, On the preparation and characterization of chars and activated carbons from orange skin, Fuel Process Technol. 91 (2010) 1345–1354, https://doi.org/10.1016/j.fuproc.2010.05.006.

[46] J. Palomo, J. Rodríguez-Mirasol, T. Cordero, Methanol dehydration to dimethyl ether on Zr-loaded P-containing mesoporous activated carbon catalysts, Materials 12 (2019) 2204–2220, https://doi.org/10.3390/ma12132204.

[47] H. Yang, R. Yan, H. Chen, D.H. Lee, C. Zheng, Characteristics of hemicellulose, cellulose and lignin pyrolysis, Fuel 86 (2007) 1781–1788, https://doi.org/10.1016/j.fuel.2006.12.013.

[48] T. Cordero, J.M. Rodriguez-Maroto, J. Rodriguez-Mirasol, J.J. Rodriguez, On the kinetics of thermal decomposition of wood and wood components, Thermochim. Acta 164 (1990) 135–144, https://doi.org/10.1016/0040-6031(90)80430-7.

[49] C. Rodríguez Correa, M. Stollovsky, T. Hehr, Y. Rauscher, B. Rolli, A. Kruse, Influence of the carbonization process on activated carbon properties from lignin

and lignin-rich biomasses, ACS Sustain Chem. Eng. 5 (2017) 8222–8233, https://doi.org/10.1021/acssuschemeng.7b01895.
[50] Y. Yamashita, K. Ouchi, Influence of alkali on the carbonization process-III: dependence on type of alkali and of alkali earth compounds, Carbon 20 (1982) 55–58, https://doi.org/10.1016/0008-6223(82)90074-4.
[51] J. Zhang, J. Liu, R. Liu, Effects of pyrolysis temperature and heating time on biochar obtained from the pyrolysis of straw and lignosulfonate, Bioresour. Technol. 176 (2015) 288–291, https://doi.org/10.1016/j.biortech.2014.11.011.
[52] M.N. Scheidema, P. Taskinen, Decomposition thermodynamics of magnesium sulfate, Ind. Eng. Chem. Res 50 (2011) 9550–9556, https://doi.org/10.1021/ie102554f.
[53] B. Souza, R. Souza, I. Santos, E. Brocchi, $MgSO_4$ carbothermic reductive decomposition to produce a highly reactive MgO powder, J. Mater. Res Technol. 9 (2020) 1847–1855, https://doi.org/10.1016/j.jmrt.2019.12.017.
[54] A. Linares-Solano, Textural characterization of porous carbons by physical adsorption of gases, Carbon Coal Gasif. (1986) 137–178, https://doi.org/10.1007/978-94-009-4382-7_5.
[55] J.L. Figueiredo, M.F.R. Pereira, M.M.A. Freitas, J.J.M. Órfão, Modification of the surface chemistry of activated carbons, Carbon 37 (1999) 1379–1389, https://doi.org/10.1016/S0008-6223(98)00333-9.
[56] J. Ruwoldt, A critical review of the physicochemical properties of lignosulfonates: chemical structure and behavior in aqueous solution, at surfaces and interfaces, Surfaces 3 (2020) 622–648, https://doi.org/10.3390/SURFACES3040042.
[57] T. Ishii, J. Ichi Ozaki, Understanding the chemical structure of carbon edge sites by using deuterium-labeled temperature-programmed desorption technique, Carbon 161 (2020) 343–349, https://doi.org/10.1016/j.carbon.2020.01.079.
[58] H. Yang, Z. Dong, B. Liu, Y. Chen, M. Gong, S. Li, H. Chen, A new insight of lignin pyrolysis mechanism based on functional group evolutions of solid char, Fuel 288 (2021) 1–8, https://doi.org/10.1016/j.fuel.2020.119719.
[59] F. Kapteijn, G. Abbel, J.A. Moulijn, CO_2 gasification of carbon catalysed by alkali metals: Reactivity and mechanism, Fuel 63 (1984) 1036–1042, https://doi.org/10.1016/0016-2361(84)90184-4.
[60] F. Kapteijn, H. Porre, J.A. Moulijn, CO_2 gasification of activated carbon catalyzed by earth alkaline elements, AIChE J. 32 (1986) 691–695, https://doi.org/10.1002/AIC.690320421.
[61] C. Moreno-Castilla, M. v López-Ramón, F. Carrasco-Marín, Changes in surface chemistry of activated carbons by wet oxidation, Carbon 38 (2000) 1995–2001, https://doi.org/10.1016/S0008-6223(00)00048-8.
[62] J.J. Ternero-Hidalgo, J.M. Rosas, J. Palomo, M.J. Valero-Romero, J. Rodríguez-Mirasol, T. Cordero, Functionalization of activated carbons by HNO_3 treatment: Influence of phosphorus surface groups, Carbon 101 (2016) 409–419, https://doi.org/10.1016/J.CARBON.2016.02.015.
[63] D. Mahon, G. Claudio, P. Eames, An experimental study of the decomposition and carbonation of magnesium carbonate for medium temperature thermochemical energy storage, Energies 14 (2021) 1316–1338, https://doi.org/10.3390/EN14051316.
[64] J.M. Rosas, J. Bedia, J. Rodríguez-Mirasol, T. Cordero, Preparation of hemp-derived activated carbon monoliths. adsorption of water vapor, Ind. Eng. Chem. Res 47 (2008) 1288–1296, https://doi.org/10.1021/IE070924W.
[65] B. Souza, R. Souza, I. Santos, E. Brocchi, $MgSO_4$ carbothermic reductive decomposition to produce a highly reactive MgO powder, J. Mater. Res Technol. 9 (2020) 1847–1855, https://doi.org/10.1016/j.jmrt.2019.12.017.
[66] M.J. Valero-Romero, F.J. García-Mateos, J. Rodríguez-Mirasol, T. Cordero, Role of surface phosphorus complexes on the oxidation of porous carbons, Fuel Process Technol. 157 (2017) 116–126, https://doi.org/10.1016/j.fuproc.2016.11.014.
[67] J.F. Moulder, W.F. Stickle, P.E.' Sobol, K.D. Bomben, Handbook of X-ray photoelectron spectroscopy, Perkin Elmer Corp. (1992).
[68] Y. Cai, Y. Pan, J. Xue, Q. Sun, G. Su, X. Li, Comparative XPS study between experimentally and naturally weathered pyrites, Appl. Surf. Sci. 255 (2009) 8750–8760, https://doi.org/10.1016/j.apsusc.2009.06.028.
[69] S. Ardizzone, C.L. Bianchi, M. Fadoni, B. Vercelli, Magnesium salts and oxide: an XPS overview, Appl. Surf. Sci. 119 (1997) 253–259, https://doi.org/10.1016/S0169-4332(97)00180-3.
[70] W. Zhang, H.L. Tay, S.S. Lim, Y. Wang, Z. Zhong, R. Xu, Supported cobalt oxide on MgO: highly efficient catalysts for degradation of organic dyes in dilute solutions, Appl. Catal. B 95 (2010) 93–99, https://doi.org/10.1016/J.APCATB.2009.12.014.
[71] M. Liu, S. Zanna, H. Ardelean, I. Frateur, P. Schmutz, G. Song, A. Atrens, P. Marcus, A first quantitative XPS study of the surface films formed, by exposure to water, on Mg and on the Mg–Al intermetallics: Al_3Mg_2 and $Mg_{17}Al_{12}$, Corros. Sci. 51 (2009) 1115–1127, https://doi.org/10.1016/J.CORSCI.2009.02.017.
[72] Z.-W. He, J. Yang, Q.-F. Lü, Q. Lin, Effect of structure on the electrochemical performance of nitrogen-and oxygen-containing carbon micro/nanospheres prepared from lignin-based composites, ACS Sustain. Chem. Eng. 1 (2013) 334–340, https://doi.org/10.1021/sc300113w.
[73] Z. Li, Y. Ge, L. Wan, Fabrication of a green porous lignin-based sphere for the removal of lead ions from aqueous media, J. Hazard Mater. 285 (2015) 77–83, https://doi.org/10.1016/J.JHAZMAT.2014.11.033.
[74] J. Pang, W.F. Zhang, J.L. Zhang, H.M. Zhang, G.P. Cao, M.F. Han, Y.S. Yang, Oxygen and nitrogen Co-enriched sustainable porous carbon hollow microspheres from sodium lignosulfonate for supercapacitors with high volumetric energy densities, ChemElectroChem 5 (2018) 1306–1320, https://doi.org/10.1002/CELC.201701384.
[75] Q.F. Lü, J.Y. Zhang, J. Yang, Z.W. He, C.Q. Fang, Q. Lin, Self-Assembled Poly(N-methylaniline)–Lignosulfonate spheres: from silver-ion adsorbent to antimicrobial material, Chem. A Eur. J. 19 (2013) 10935–10944, https://doi.org/10.1002/CHEM.201204113.
[76] J. Yang, Y.C. Ching, C.H. Chuah, Applications of lignocellulosic fibers and lignin in bioplastics: a review, Polymers 11 (2019) 1–26, https://doi.org/10.3390/polym11050751.
[77] N. Tancredi, T. Cordero, J. Rodriguez-Mirasol, J.J. Rodriguez, CO_2 gasification of eucalyptus wood chars, Fuel 75 (1996) 1505–1508, https://doi.org/10.1016/0016-2361(96)82641-X.
[78] F. Marquez-Montesinos, T. Cordero, J. Rodriguez-Mirasol, J.J. Rodriguez, CO_2 and steam gasification of a grapefruit skin char, Fuel 81 (2002) 423–429, https://doi.org/10.1016/S0016-2361(01)00174-0.
[79] S. Porada, A. Rozwadowski, K. Zubek, Studies of catalytic coal gasification with steam, Pol. J. Chem. Technol. 18 (2016) 97–102, https://doi.org/10.1515/pjct-2016-0054.
[80] P.J.M. Carrott, Suhas, M.M.L. Ribeiro Carrott, C.I. Guerrero, L.A. Delgado, Reactivity and porosity development during pyrolysis and physical activation in CO_2 or steam of kraft and hydrolytic lignins, J. Anal. Appl. Pyrolysis 82 (2008) 264–271, https://doi.org/10.1016/j.jaap.2008.04.004.
[81] E. Gonzalez-Serrano, T. Cordero, J. Rodríguez-Mirasol, J.J. Rodríguez, Development of porosity upon chemical activation of kraft lignin with $ZnCl_2$, Ind. Eng. Chem. Res 36 (1997) 4832–4838, https://doi.org/10.1021/IE970261Q.
[82] J. Pang, W. Zhang, J. Zhang, G. Cao, M. Han, Y. Yang, Facile and sustainable synthesis of sodium lignosulfonate derived hierarchical porous carbons for supercapacitors with high volumetric energy densities, Green. Chem. 19 (2017) 3916–3926, https://doi.org/10.1039/c7gc01434a.
[83] A. Corma, S. Iborra, A. Velty, Chemical routes for the transformation of biomass into chemicals, Chem. Rev. 107 (2007) 2411–2502, https://doi.org/10.1021/cr050989d.
[84] K.J. Klabunde, J. Stark, O. Koper, C. Mohs, D.G. Park, S. Decker, Y. Jiang, I. Lagadic, D. Zhang, Nanocrystals as stoichiometric reagents with unique surface chemistry, J. Phys. Chem. 100 (1996) 12142–12153. ⟨https://pubs.acs.org/sharingguidelines⟩.
[85] V.K. Díez, C.A. Ferretti, P.A. Torresi, C.R. Apesteguía, J.I. di Cosimo, Effect of MgO activation conditions on its catalytic properties for base-catalyzed reactions, Catal. Today 173 (2011) 21–27, https://doi.org/10.1016/J.CATTOD.2011.02.060.
[86] T. Kanno, M. Kobayashi, 2.14 evaluation of basicity of alkali metal-doped MgO in the scope of change of carbonate species, Stud. Surf. Sci. Catal. 90 (1994) 207–212, https://doi.org/10.1016/S0167-2991(08)61821-2.
[87] J.I. di Cosimo, V.K. Díez, C. Ferretti, C.R. Apesteguía, Basic catalysis on MgO: generation, characterization and catalytic properties of active sites, Catalysis 26 (2014) 1–28, https://doi.org/10.1039/9781782620037-00001.
[88] A. Gervasini, J. Fenyvesi, A. Auroux, Study of the acidic character of modified metal oxide surfaces using the test of isopropanol decomposition, Catal. Lett. 43 (1997) 219–228, https://doi.org/10.1023/A:1018979731407.
[89] A. Auroux, A. Gervasini, Microcalorimetric study of the acidity and basicity of metal oxide surfaces, J. Phys. Chem. A 94 (1990) 6371–6379, https://doi.org/10.1021/J100379A041.
[90] C.S. Narasimhan, C.S. Swamy, Studies on the decomposition of isopropyl alcohol on Mg $Al_{2-x}Fe_xO_4$, Appl. Catal. 2 (1982) 315–328, https://doi.org/10.1016/0166-9834(82)80077-8.
[91] E. Suzuki, S. Idemura, Y. Ono, Catalytic conversion of 2-propanol and ethanol over synthetic hectorite and its analogues, Appl. Clay Sci. 3 (1988) 123–134, https://doi.org/10.1016/0169-1317(88)90012-9.
[92] M.A. Aramendía, V. Borau, C. Jiménez, J.M. Marinas, A. Porras, F.J. Urbano, Magnesium oxides as basic catalysts for organic processes study of the dehydrogenation-dehydration of 2-propanol, J. Catal. 161 (1996) 829–838, https://doi.org/10.1006/jcat.1996.0246.
[93] V.K. Díez, C.R. Apesteguía, J.I. di Cosimo, Acid–base properties and active site requirements for elimination reactions on alkali-promoted MgO catalysts, Catal. Today 63 (2000) 53–62, https://doi.org/10.1016/S0920-5861(00)00445-4.
[94] M.C.G. Albuquerque, D.C.S. Azevedo, C.L. Cavalcante, J. Santamaría-González, J. M. Mérida-Robles, R. Moreno-Tost, E. Rodríguez-Castellón, A. Jiménez-López, P. Maireles-Torres, Transesterification of ethyl butyrate with methanol using MgO/CaO catalysts, J. Mol. Catal. A Chem. 300 (2009) 19–24, https://doi.org/10.1016/j.molcata.2008.10.033.
[95] T. Wang, G. Wu, N. Guan, L. Li, Nitridation of MgO-loaded MCM-41 and its beneficial applications in base-catalyzed reactions, Microporous Mesoporous Mater. 148 (2012) 184–190, https://doi.org/10.1016/j.micromeso.2011.07.024.